

Construction of Eukaryotic Cell Biomimetics: Hierarchical Polymersomes-in-Proteinosome Multicompartment with Enzymatic Reactions Modulated Protein Transportation

Ping Wen, Xueyi Wang, Silvia Moreno, Susanne Boye, Dagmar Voigt, Brigitte Voit, Xin Huang,* and Dietmar Appelhans*

The eukaryotic cell is a smart compartment containing an outer permeable membrane, a cytoskeleton, and functional organelles, presenting part structures for life. The integration of membrane-containing artificial organelles (=polymersomes) into a large microcompartment is a key step towards the establishment of exquisite cellular biomimetics with different membrane properties. Herein, an efficient way to construct a hierarchical multicompartment composed of a hydrogel-filled proteinosome hybrid structure with an outer homogeneous membrane, a smart cytoskeleton-like scaffold, and polymersomes is designed. Specially, this hybrid structure creates a micro-environment for pH-responsive polymersomes to execute a desired substance transport upon response to biological stimuli. Within the dynamic pH-stable skeleton of the protein hydrogels, polymersomes with loaded PEGylated insulin biomacromolecules demonstrate a pH-responsive reversible swelling-deswelling and a desirable, on-demand cargo release which is induced by the enzymatic oxidation of glucose to gluconic acid. This stimulus responsive behavior is realized by tunable on/off states through protonation of the polymersomes membrane under the enzymatic reaction of glucose oxidase, integrated in the skeleton of protein hydrogels. The integration of polymersomes-based hybrid structure into the proteinosome compartment and the stimuli-response on enzyme reactions fulfills the requirements of eukaryotic cell biomimetics in complex architectures and allows mimicking cellular transportation processes.

compartment-defining barrier, cytoskeleton, and intracellular organelles where specific metabolic activities take place widely.^[1] The cytoskeleton plays a crucial role in resisting cell deformation and migration, intracellular cargo transport, organelle localization and fixing;^[2] surrounded by unique membrane structure, the intracellular organelle provides a space for a series of biological processes, such as response behaviors to environmental stimuli and specific metabolic activities.^[3] To deeply investigate and profoundly understand the cell structures or functions of such highly orchestrated microstructured assemblies, recently, numerous and various micro-sized (multi)compartments have been created including polymersomes,^[4–6] liposomes,^[7] colloidosomes,^[8] coacervates,^[9] and proteinosomes,^[10] and other (multi)compartments of them.^[11–15] In order to prepare simplified cellular models certain cellular properties and behaviors have been successfully installed such as, modulated cascade enzymatic reaction,^[16] enhanced protein refolding,^[17] cytoskeletal assembly,^[18] membrane fusion,^[14,19] phagocytosis,^[20] and predatory behavior.^[21–22] However, such simple cell-sized models are difficult to be used to study a series of complicated biological behaviors and activities. To understand the intracellular communications and processes of (multi)compartmentalized

1. Introduction

As a remarkably complex bioreactor, eukaryotic cells are composed of an outer permeable membrane as their

P. Wen, Prof. X. Huang
MIIT Key Laboratory of Critical Materials Technology for New Energy Conversion and Storage
School of Chemistry and Chemical Engineering
Harbin Institute of Technology (HIT)
Harbin 150001, P. R. China
E-mail: xinhuang@hit.edu.cn

 The ORCID identification number(s) for the author(s) of this article can be found under <https://doi.org/10.1002/smll.202005749>.

© 2020 The Authors. Small published by Wiley-VCH GmbH. This is an open access article under the terms of the Creative Commons Attribution-NonCommercial-NoDerivs License, which permits use and distribution in any medium, provided the original work is properly cited, the use is non-commercial and no modifications or adaptations are made.

DOI: 10.1002/smll.202005749

X. Wang, Dr. S. Moreno, Dr. S. Boye, Prof. B. Voit, Dr. D. Appelhans
Leibniz-Institut für Polymerforschung Dresden e.V.
Hohe Straße 6, D-01069 Dresden, Germany
E-mail: applhans@ipfdd.de
X. Wang, Prof. B. Voit
Chair of Organic Chemistry of Polymers
Technische Universität Dresden
D-01062 Dresden, Germany
Dr. D. Voigt
Institute for Botany
Faculty of Biology
Technische Universität Dresden
D-01062 Dresden, Germany

eukaryotic cells, smaller organelle compartments are located inside the cell allowing their tracking, positional assembly, and processes in different compartments. This thoroughly provides cells with spatiotemporal control over metabolic reactions. Multi-compartmentalized microstructured assemblies have demonstrated their potential application in the field of drug delivery, drug screening, microreactors, biomaterials, etc.^[13,23,24] They might be used for advancing cellular model design to delineate some complex multistep processes of modern living cell.^[13,25–27]

Recently, combining the self-assembly of different components, for example through the use of Pickering emulsion or the direct encapsulation of small microcompartments into a large one, various multicompartment systems have been successfully created including liposomes in liposomes,^[28] polymersomes in polymersomes,^[29] proteinosomes in proteinosome^[24,30] and hybrid multicompartment system such as liposomes in polymersomes^[31] and polymersomes in coacervate.^[32–33]

The aim of the study was to build cell-like multicompartmental micro-sized structures (CMMS). **Figure 1** highlights the approach of our study. For this, CMMS should be characterized by multiple orthogonal-responsive membranes leading to different permeability characteristics of the outer membrane (MWCO up to 70 kDa) for CMMS and of pH-responsive polymersomes membrane with permeable membrane under acidic pH and collapsed membrane at $\text{pH} \geq 7$.^[34] Furthermore, membrane-bounded and confined polymersomes are needed as artificial organelles for the pH-dependent storage and release of biological (macro)molecules. Moreover, a dynamically controlled skeleton of CMMS is highly required for the spatial organization of resided enzymes and biological stimuli-responsive artificial organelles. This should undoubtedly allow a synergistic modulation of substance transportation to the extracellular environment or certain complex cascade enzyme reactions.

Here, we demonstrate the concept of CMMS using the highly efficient Pickering emulsion method^[10] for the incorporation of

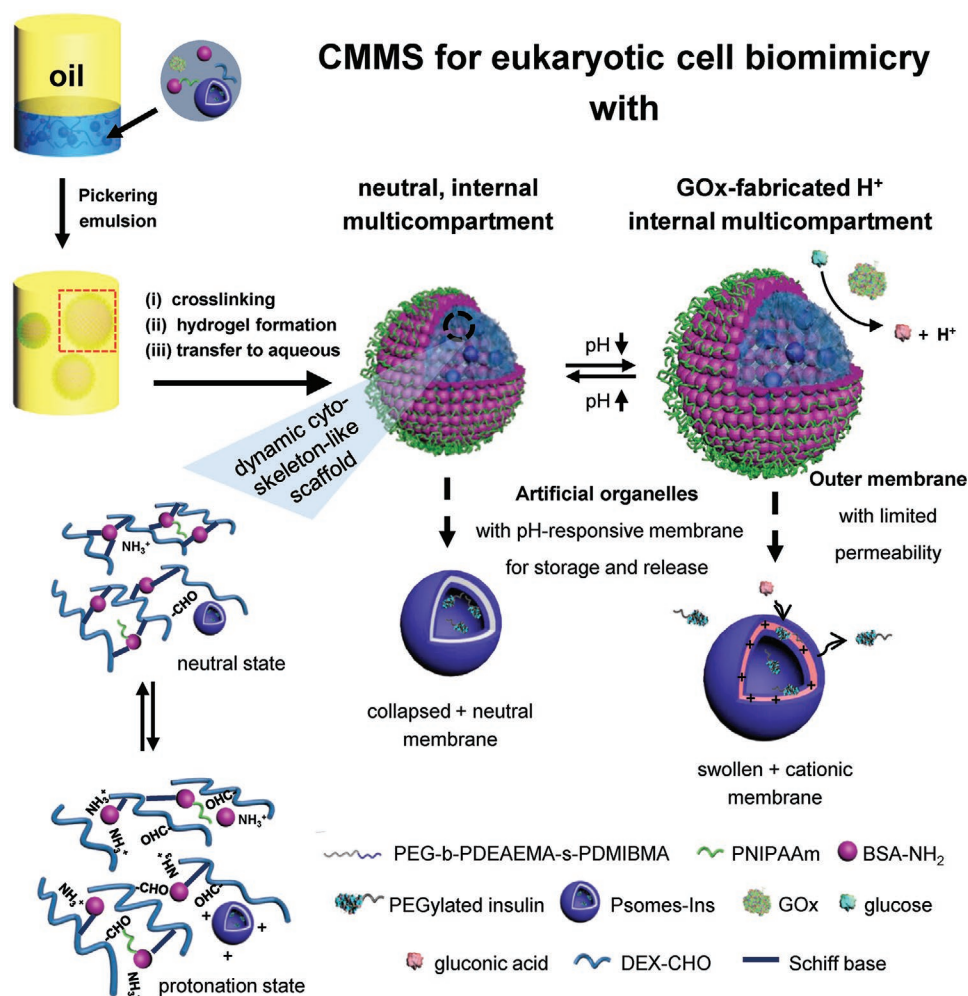


Figure 1. Schematic representation of the construction of dynamic and feedback-controlled eukaryotic cell biomimetics with orthogonal-responsive membranes by Pickering emulsion method: pH- and glucose-responsive polymersomes-in-proteinosome as cell-like multicompartmental micro-sized structures (CMMS). pH-dependent release of PEGylated insulin from artificial organelles (=polymersomes) stimulated by enzyme reaction. Cargo release depends on the expansion–contraction of protein hydrogel (=cytoskeleton-like scaffold) and ON-OFF transition of artificial organelle membrane in proteinosome. Skeleton-like scaffold in the inner compartment of proteinosomes (SLSP). GOx is also integrated in the SLSP through non-covalent interactions, meaning within CMMS. Further details on the locations of PEGylated insulin is given in Figure 4a.

PEGylated-insulin-(PEG-Ins)-loaded polymersomes (Psomes-Ins) and glucose oxidase (GOx) into a protein hydrogel-filled proteinosome^[19] (Figure 1). The use of PEG-Ins in biomimetic eukaryotic cell is motivated that pure hormone insulin (Ins) efficiently reduces the glucose level in the blood. However, their colloidal stability is limited in different solutions but also, for example, when amyloidosis, meaning pathological protein deposition in human organs, is occurring.^[35–36] Thus, the easy aggregation of Ins limits any biological experiments and further applications. Finally, we would like to simulate pancreatic beta cells as simple showcase for CMMS.

The protein hydrogel inside the proteinosomes is composed of cationized BSA and aldehyde-dextran and is considered to be an artificial cytoskeleton due to its dynamic pH-stable behavior.^[19] Thus, it avoids undesired polymersome aggregation and leads to their even distribution within the proteinosomes. On the other hand, this skeleton-like protein hydrogel also protects entrapped enzymes from misfolding and/or denaturation under the external stimuli.^[37] Significantly, for inducing biological stimuli, the oxidation reaction of glucose catalyzed by the GOx has been preferentially carried out inside the proteinosomes for producing an acid microenvironment inside the CMMS. This leads to the synchronized swelling of skeleton-like scaffold and artificial organelle (Psomes-Ins) within CMMS. Thus, the release of PEG-Ins from artificial organelles could be triggered by pH and electrostatic interactions between PEG-Ins and membrane of the artificial organelle, regardless of the pH of the outer aqueous solution.

2. Results and Discussion

2.1. Construction of Proteinosome with Skeleton-Like Protein Hydrogel Scaffold

As described in previous papers, proteinosomes are capable of high cargo loading, demonstrate size-selective permeability of their membrane, allow multicompartments formation, and exhibit thermo-responsive properties.^[10,18] Due to extra thin semi-permeable membrane and large hollow lumen, empty proteinosome can easily collapse under the air drying condition and can also break by external mechanical stimuli.^[19] To improve the mechanical stability of proteinosomes, their outer membrane can be stabilized by an outer inorganic layer or by the direct formation of hydrogel inside proteinosomes.^[18,38] For our study, the latter approach was used to fabricate mechanically stable microcompartments. Thus, protein hydrogel prepared by aldehyde-functionalized dextran (DEX-CHO) and water-soluble cationized bovine serum albumin (BSA-NH₂) is used as skeleton-like scaffold in the inner compartment of proteinosomes (SLSP) (Figures 2a and 7b–d). The protein hydrogel in SLSP is thoroughly cross-linked by Schiff base (=imine) linkages composed of aldehyde and amine groups (Figure 1) and has a representative 3D network shown in the scanning electron microscopic (SEM) image (Figure 2b). In particular, this skeleton-like protein hydrogel scaffold in SLSP can well maintain the spherical architecture (Figure 2c), which is needed for the final fabrication of CMMS. Besides, the SEM image of the intact single sphere structure (Figure 2c), obtained after critical

point drying under vacuum conditions, also proves that the protein hydrogel scaffold with its cytoskeleton-resembling characteristics can undeniably support the mechanical properties of proteinosomes. Furthermore, SLSP outlines a porous structure with larger adsorption and/or loading capacity (Figure S3, Supporting Information) in comparison to that of empty proteinosomes (Figure S2, Supporting Information). This leads to a different diffusion within the SLSP compared to empty compartments (Figure S3, Supporting Information) allowing a retarded release of small proteins such as myoglobin from SLSP which had been encapsulated in SLSP during the Pickering emulsion process (Figure S4, Supporting Information).

Importantly, we could demonstrate that the pH-responsive SLSP outlines the desired (cyclic) pH stability, induced by GOx-mediated pH drop (Figure 2e–g) and repeating acid and base addition (Figure 2h–k). Thus, the swelling and shrinking SLSP can keep its integrity smoothly governed by the dynamic chemical equilibrium between free aldehyde and amine groups and formed imine crosslinking points.^[19,37] To avoid a complete disassembly of the imine-based protein hydrogel in SLSP, slight excess glutaraldehyde (0.5% mass ratio) was added which promoted the presence of at least partial imine crosslinking points in the SLSP even in the protonated state. Due to the partial opening of the imine crosslinking points upon protonation, there is a 21% volume increase of SLSP by changing pH from 8 to 5 (Figure 2h–k; details shown in the Supporting Information). Finally, the desired GOx/glucose-mediated pH drop in the inner microenvironment of CMMS was also validated through encapsulation of GOx, glucose, as well as pH indicator phenol red in SLSP and following pH changes in the microcompartment upon GOx enzyme activity (Figure 2e–g). As proposed, the GOx/glucose-mediated acidic microenvironment can be fabricated selectively and spatially confined within SLSP. The pH drop from pH 8 to pH 6.5 is visible through the color change of indicator phenol red from light red to yellow in comparison with no color changes in the outer aqueous solution (Figure 2e–g).

2.2. Construction of PEGylated Insulin Loaded Polymersomes

To construct functional CMMS, pH-responsive and photocrosslinked polymersomes (Psomes)^[34,39–43] are used as artificial organelles for storage and release of the biomacromolecule PEG-Ins inside the CMMS. From previous studies, our selected Psomes are attributed with the following characteristics: a pH-sensitive switchable permeability of the polymersome's membrane and thus a pH-dependent release and storage of biologically-active (macro)molecules, and a high mechanical stability against shear forces.^[34,39–43] In order to better understand the physico-chemical, morphological, and structural characteristics of Psomes-Ins, respective empty Psomes were used as reference. Further details for the synthesis of empty Psomes, including the synthesis of amphiphilic block copolymer (BCP-A = PEG-b-PDEAEMA-s-PDMIBMA in Figure 1), are presented in the Supporting Information.

To avoid dimer or multimer formation of Ins around their isoelectric point (pI 5.3), PEG modification of Ins promotes a longer life time of non-aggregated Ins under selected conditions. Thus, PEG-Ins was synthesized for

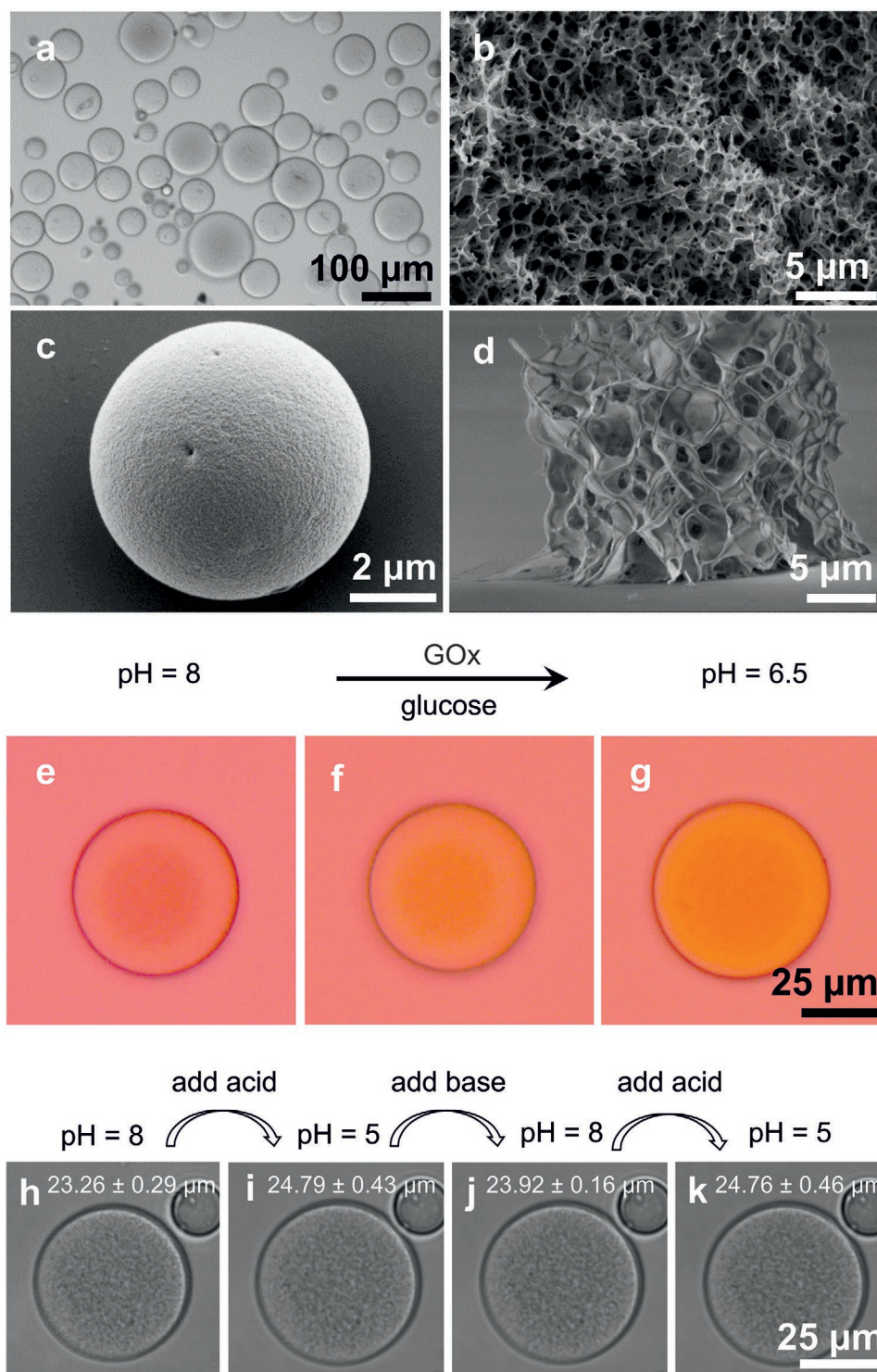


Figure 2. Characterization of proteinosomes with internal protein hydrogel as skeleton-like scaffold in the inner compartment of proteinosome (=SLSP). a) The light microscopy image of SLSP with average size distribution around 20 μm . b) SEM image showing the porous cytoskeleton-like scaffold of protein hydrogel. c) SEM image of SLSP and d) cryo-SEM image of proteinosome with SLSP under high vacuum condition (leading to the destruction of spherical structures under (c)). e–g) Light microscopy images for pH-sensitivity of proteinosome with SLSP and incorporated GOx. The pH indicator phenol red exhibits a gradual transition from light red to yellow over the pH range from 8 to 6.5 (duration of 1 h), mediated by GOx-glucose enzyme reaction. Thus, protons are delivered by gluconic acid (=oxidized glucose). h–k) Light microscopy images for the reversible swelling properties of proteinosome with SLSP and GOx between pH 5 and pH 8, the swelling ratio ($V_{\text{pH } 5}:V_{\text{pH } 8} = 7973 \mu\text{m}^3:6586 \mu\text{m}^3$) is around 1.21. The mean sizes were calculated by counting 40 particles in the case of (h–k).

our study (Figure S7a; further details in the Supporting Information), resulting in the attachment of 1–2 PEG chains per Ins (Figure S7b, Supporting Information).^[44] Circular dichroism spectra confirm that the tertiary structure of Ins in aqueous solution is essentially conserved after PEG chain modification (Figure 3a). The colloidal stability of Ins and PEG-Ins in physiological environment was assessed by carrying out pH-dependent dynamic light scattering (DLS) over time. As it could be shown, PEG-Ins (0.2 mg mL⁻¹) remains stable when it is incubated for more than 24 h in 10 mM PBS buffer solution at pH values near the isoelectric point of PEG-Ins and up to neutral pH (pH 5.5, 6.5, and 7.4) (Figure 3b; Figure S8, Supporting Information). In contrast, native Ins tends to form larger aggregates at pH values around isoelectric point (Figure 3c), especially between pH 5 and 6.5 (Figure S9, Supporting Information). In comparison to pure Ins, the isoelectric point (pI) of PEG-Ins slightly shifts to lower pH value (≈5; Figure 3c). Finally, this also implies that anionic PEG-Ins (above pI 5) can easily undergo ionic interactions with any cationic biological/polymeric materials, when used in any biological and/or loading, storage, and release processes.

It is well known that Psomes provide the possibility to load hydrophilic and hydrophobic cargo such as proteins, oligo/poly-nucleic acids, nanoparticles and protein mimics in the hydrophobic membrane and/or hydrophilic lumen.^[34,39,45–49] Following our previously reported in situ encapsulation method during the formation of Psomes,^[39] Psomes-Ins had been obtained after hollow fiber filtration (HFF) purification process (further details in the Supporting Information). Loading efficiency of PEG-Ins in Psomes-Ins is about 41.7% (Figure S10, Supporting Information; it is calculated using RBITC labeled PEG-Ins).

Posomes-Ins show similar (structural) characteristics as found for empty Psomes (Figures 3d–f and 5a,b; Figures S6 and S11, Supporting Information). Validated from cryo-TEM study (Figure S6, Supporting Information), the diameter at pH 8 decreases from 71.7 nm (empty Psomes) to 63.8 nm (Posomes-Ins), while the Psomes membrane thickness increases from 15.4 nm (empty Psomes) to 17.3 nm (Posomes-Ins). This is caused by the obvious partial incorporation of PEG-Ins in Psomes membrane, while a minor attachment of PEG-Ins on Psomes surface is also possible. Generally, Psomes-Ins outline a slightly lower surface charge than empty Psomes between pH 5 and pH 6.5 (Figure 3e).

Furthermore, asymmetrical flow field flow fractionation with light scattering detection (AF4-LS) supported the understanding of the in situ loading process of PEG-Ins during Psomes formation. The above-mentioned size reduction of Psomes-Ins during the in situ loading is also confirmed by AF4-LS (Figure S24, Supporting Information). AF4 enables a gentle separation of free PEG-Ins and Psomes-Ins (Figures S24 and S25a, Supporting Information) for unpurified Psomes-Ins sample at pH 8. Thus, a quantification of the isolated PEG-Ins amount, using the concentration sensitive UV detection (Figure S23 and Table S3, Supporting Information), is possible. After HFF purification of the Psomes-Ins sample, a certain amount of PEG-Ins is released from Psomes-Ins at pH 8 (details on AF4 study are given in the Supporting Information, Figures S25a and S26). Slight influences of HFF purification on the conformation of the Psomes-Ins can be observed, revealing

slightly different scaling parameters (Figure S25b, Supporting Information). The comparison of apparent density before and after HFF shows a decrease due to removal of PEG-Ins located on Psomes surface and membrane (Figure S25c, Supporting Information). The ρ parameter (R_g/R_h) of around 1 reveals the shape of a soft sphere at the main fraction of Psomes-Ins and concentration maximum (Figure S25d, Supporting Information). The AF4 study also confirms the results obtained by DLS and cryo-TEM.

In summary, the key characteristics of Psomes are only slightly/marginally changed in Psomes-Ins: i) slight decrease of pH* (half power of swelling or semi-swollen state) from 6.4 to 6.2 (Figure 3f); ii) slight drop of collapsing point of Psomes membrane (state for impermeable membrane) from about pH 7.0 to around pH 6.6; iii) cyclic reversible swelling and shrinking of Psomes-Ins (Figure 3d). Thus, Psomes-Ins behaves like other protein-loaded Psomes.^[39,50] This fact allowed the next series of experiments for validating the release of PEG-Ins under physiological environments.

2.3. Study of the Release of PEGylated Insulin from Psomes-Ins

It was our goal to provide an acidic microenvironment in our CMMS by the enzymatic reaction of GOx with glucose forming gluconic acid as product and to induce by that transport processes, for example, the release of PEG-Ins, from the inner organelle mimics, our Psomes-Ins. Thus, to verify PEG-Ins release behavior from Psomes-Ins under specific conditions, the following release experiments were carried out: Psomes-Ins stock solutions (0.2 mg mL⁻¹; using small dialysis tube) were dialyzed against i) 10 mM PBS buffer (pH 7.4, 6.5, and 5.5), ii) aqueous gluconic acid solutions (0, 1, and 10 mg mL⁻¹ in 10 mM PBS buffer), and iii) glucose (10 mg mL⁻¹) and GOx (0.2 mg mL⁻¹) and the amount of released PEG-Ins was verified by fluorescence spectroscopy. For pH-dependent release of PEG-Ins in PBS buffer at pH 5.5 (Figure 4b), the cumulative release of PEG-Ins is in a lower degree compared to that at pH 6.5 and 7.5. Here, the release at pH 5.5 is hindered by stronger electrostatic interactions between protonated Psomes membrane (Figure 3e) and the negatively charged PEG-Ins (Figure 3c) in spite of thoroughly swollen Psomes membrane (Figure 3f). Considering the “off state” of Psomes membrane in PBS buffer above pH 6.5 (Figure 3f) the slightly increasing release rates of PEG-Ins are reasonable due to weakening electrostatic interactions (Figure 3e). In contrast to pH 5.5 and 6.5, the highest release rate is observed at pH 7.4 despite the presence of collapsed Psomes’ membrane (Figure 4b). This smoothly implies that PEG-Ins cannot be retained at this membrane state under these specific conditions. Interestingly, the release rates of PEG-Ins increases with raising concentration of gluconic acid (Figure 4c). It is postulated that gluconic acid influences the electrostatic interactions between the cationic amino groups of Psomes membrane and the anionic PEG-Ins. Gluconic acid screens the cationic charge of Psomes membrane which is then no longer able to undergo electrostatic interactions as known in the case of pH-dependent release, especially at pH 5.5 (Figure 4b). Thus, the increased release of PEG-Ins is obvious under these specific conditions (Figure 4c), resembling

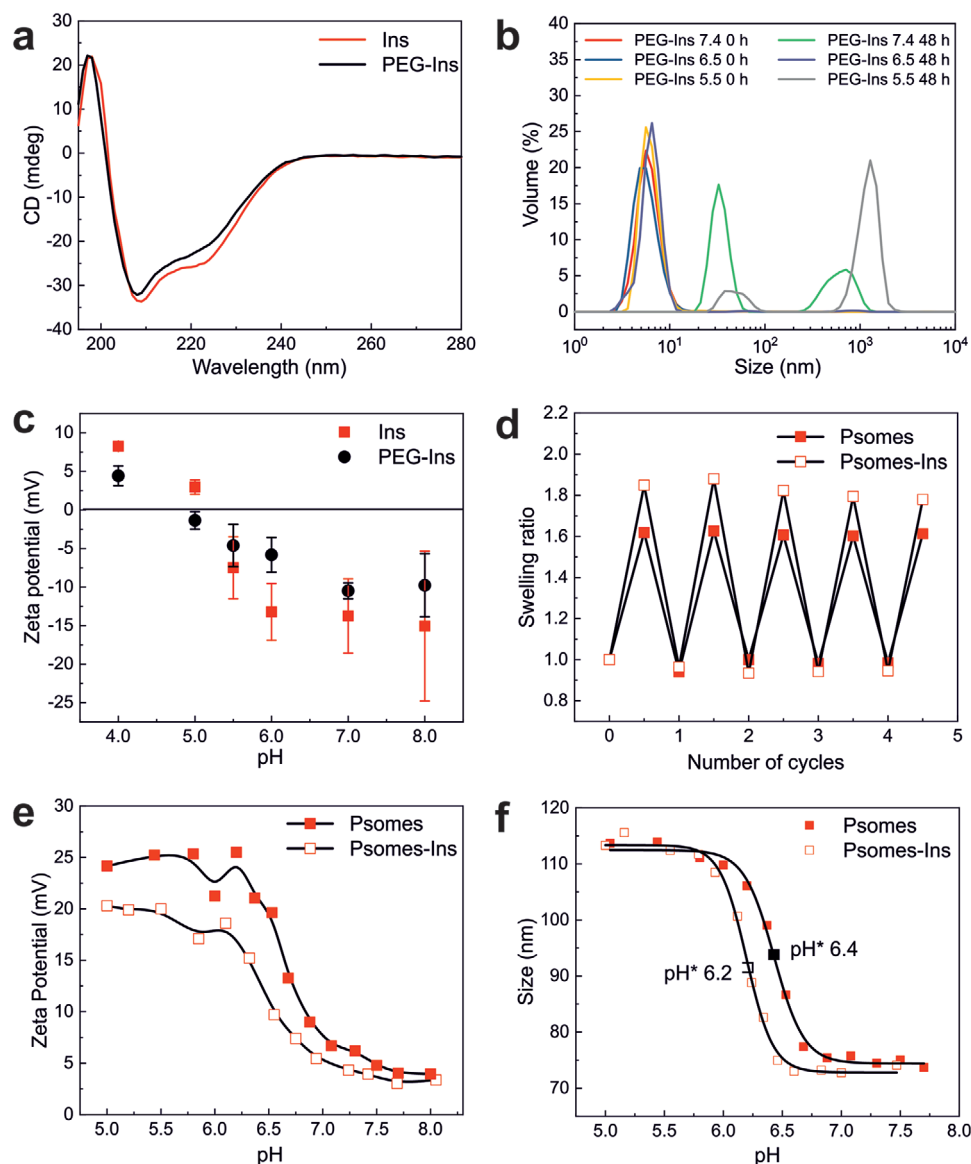


Figure 3. a) Near-UV circular dichroism spectra of pure insulin (Ins) and PEGylated insulin (PEG-Ins). b) Time-dependent size distributions of PEG-Ins carried out by DLS in the solution of 1 mM PBS at pH 7.4, 6.5, and 5.5, respectively. c) pH-dependent zeta potential changes of native Ins and PEG-Ins. Data are presented as mean values \pm SD; error bars indicate standard deviations ($n = 3$). d) Cyclic pH-switches of polymersomes (Posomes) and PEG-Ins-loaded polymersome (Posomes-Ins) between pH 5 and pH 8 determined by DLS. e) pH-dependent zeta potential curves of empty Psomes and Psomes-Ins. f) pH-dependent DLS titration curves of empty Psomes and Psomes-Ins for determining the critical pH value (pH*).

physiological blood conditions at which glucose was substituted by gluconic acid.^[36]

For the final adaptation of acidic microenvironment within CMMS high glucose concentration (10 mg mL^{-1}), GOx (0.2 mg mL^{-1}), and Psomes-Ins ($C_{\text{Posomes-Ins}} = 1 \text{ mg BCP mL}^{-1}$ and $0.2 \text{ mg PEG-Ins mL}^{-1}$; used as purified solution) were mixed in order to validate the release of PEG-Ins under physiological conditions being present in a human body (Figure 4d; analyzed by Figure S12, Supporting Information). It should be clarified whether the biological stimulus GOx/glucose is already suited to produce a lower acidic environment at which Psomes membrane is protonated for inducing the desired release of PEG-Ins from Psomes-Ins. As shown in Figure 4d,

the pH changes continuously to lower values due to the increased production of gluconic acid during the enzymatic reaction and accordingly PEG-Ins is released. In the first stage, between pH 7.5 and 7.0 the PEG-Ins is released at a relatively fast speed due to weak electrostatic interaction between PEG-Ins and the Psomes' membrane. Afterwards, with decreasing pH over time, the release curve turns to a slower release profile of PEG-Ins due to simultaneous production of protons for lower pH, protonation of Psomes' membrane and electrostatic interactions of gluconic acid with cationic Psomes' membrane. For example, lowering the pH further from 6 to pH 5, the release rate is slower but the amount of released PEG-Ins again increases, first, because now the Psomes'

a Behavior of pH-dependent release of PEG-Ins (Δ) different to gluconic acid- and GOx/glucose-induced release

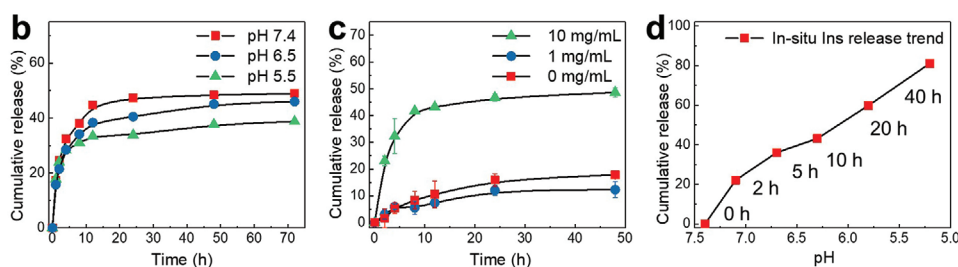
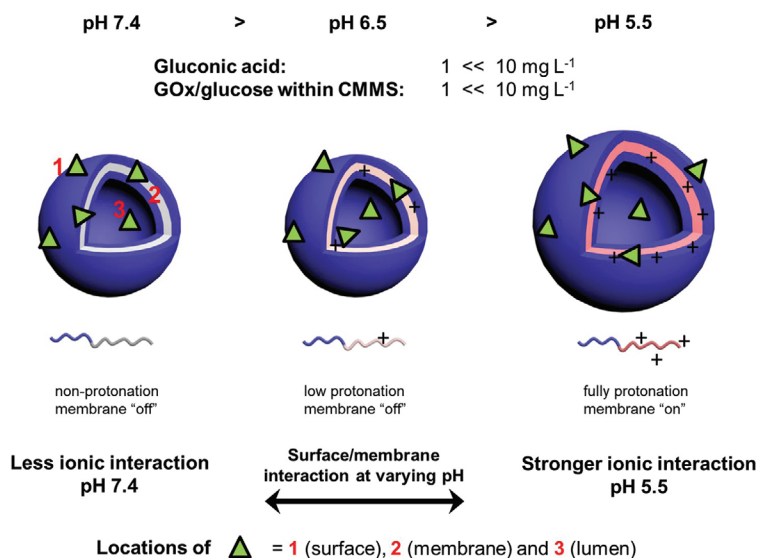


Figure 4. a) Comparison of PEG-Ins (RBITC labeled PEGylated insulin) release from Psomes-Ins induced by proton, gluconic acid, and GOx/glucose source. Schematic illustration of locations of PEG-Ins and charge of Psomes' membrane at different protonation state. Release of PEG-Ins is strongly influenced by the microenvironment. For example, charge of Psomes membrane is screened by gluconic acid; further details in text. b) Cumulative PEG-Ins release from Psomes-Ins induced by dialyzing Psomes-Ins solution in 10 mM PBS buffer at pH 7.4, 6.5, and 5.5. c) Cumulative PEG-Ins release from Psomes-Ins induced by dialyzing Psomes-Ins solution in 10 mM PBS buffer in the presence of 0, 1, and 10 mg mL⁻¹ of gluconic acid. Data are presented as mean values \pm SD; error bars indicate standard deviations ($n = 3$). d) PEG-Ins release from Psomes-Ins in the presence of high glucose concentration (10 mg mL⁻¹) and glucose oxidase (GOx) to imitate the final release trend of PEG-Ins from CMMS.

membrane is fully swollen, and second, the electrostatic interactions in the Psomes' membrane are screened by the increasing concentration of the produced gluconic acid (Figure 4d). The retarded release at lower pH is not completely understood and needs more detailed investigations. Overall, we can state the adaptation to generate potential acidic microenvironment in CMMS through an enzymatic reaction works well.

2.4. Construction of Polymersomes-in-Proteinosome Hybrid Multicompartment

In the next step, the Psomes-Ins were encapsulated into "empty" proteinosome compartments using the easily applicable Pickering emulsion method which almost leads to a high loading efficiency of various components.^[10] Thus, polymersomes-in-proteinosome multicompartment structures have been obtained and were characterized (Figure 5d; Figures S13–S15, Supporting Information). The successful encapsulation of the

Posomes-Ins inside the proteinosome is clearly identified from the TEM measurement (Figure 5d; Figure S13, Supporting Information). In comparison to empty proteinosomes with their very transparent protein membrane, the Psomes-Ins locations (dark spheres) inside proteinosomes can be readily visualized. In contrast to pure proteinosomes which show high colloidal stability in 10 mM PBS buffer at pH 7.5, 6.5, and 5.5 over 7 days (Figure S14, Supporting Information), slight aggregation of dye-labeled Psomes-Ins inside the proteinosomes, probably favored by non-covalent interactions of involved components in combination with glue properties of salt solutions, is visible after 7 days. In this regard one has to take into account, based on the study outlined above (Figure 4b), that under the storage conditions PEG-Ins will be slowly released after days and can also form aggregated particles over time (Figure S8, Supporting Information). This implies that the lower colloidal stability of Psomes-Ins may be influenced by aggregated PEG-Ins in the confinement of proteinosomes in 10 mM PBS solutions (Figure S15, Supporting Information).

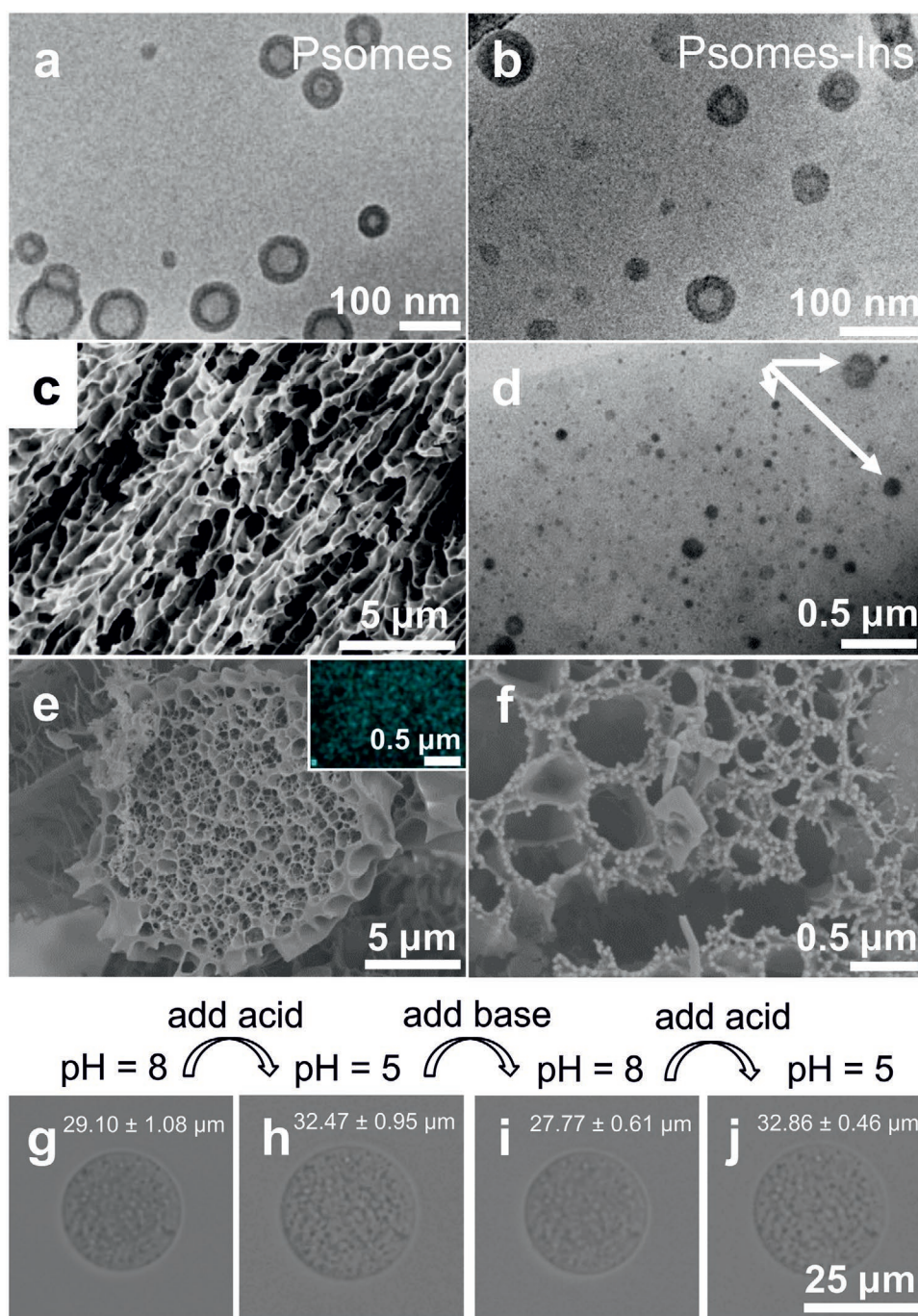


Figure 5. Characterization of cell-like multicompartmental micro-sized structures (CMMS with Psomes and without GOx). a) Cryo-TEM micrographs of empty Psomes (diameter: averaged 71.7 nm ($N = 200$), membrane thickness: averaged 15.4 nm ($N = 100$)) and b) PEG-Ins-loaded polymersomes (Psomes-Ins) (diameter: averaged 63.8 nm ($N = 200$), membrane thickness: averaged 17.3 nm ($N = 100$)) in 10 mM PBS buffer at pH 8). c) SEM image of the inner part of proteinosome with SLSP and Psomes (1 mg mL^{-1}); polymersomes are too small to be seen. d) TEM image of the inner part close to its surface for polymersomes-(Psomes)-loaded proteinosomes without SLSP after staining with uranyl acetate (white arrows point to the Psomes). e) Cryo-SEM image of half sphere of CMMS with Psomes; inset top right: sulfur elemental mapping analysis of RBITC-labeled PEG-Ins-loaded Psomes in CMMS and f) magnification image of CMMS with Psomes of (e), demonstrating the small intact and well distributed Psomes on the skeleton. g–j) Cyclic pH-switches of CMMS with Psomes between pH 5 and pH 8, the swelling ratio ($V_{\text{pH } 5} : V_{\text{pH } 8} = 17\,915 \mu\text{m}^3 : 12\,896 \mu\text{m}^3$) is around 1.39. The mean sizes were calculated by counting 40 particles for each case (Figure 2g–j).

The successful establishment of polymersomes-in-proteinosomes multicompartment structures motivated us to realize the desired cell biomimetics of CMMS, first without

the enzyme GOx. Following the procedure of SLSP by Pickering emulsion method, the polymersomes were incorporated into SLSP to realize CMMS. This multicompartment

structure exhibits excellent structural stability and integrity under neutral and acidic conditions for more than 15 days (Figure S16, Supporting Information). The morphology of the multicompartiment structure was examined by confocal fluorescence microscopy (CLSM), SEM, and cryo-SEM combined with EDX measurements. Because of the small size of the polymersomes, after their loading in CMMS there is no obvious difference from the macroscopic view compared with that of SLSP (Figures 2b and 5c; Figures S17–S19, Supporting Information). However, from the cryo-SEM images combined with sulfur EDX line scan (Figure 5e), one can see the homogeneous distribution of the polymersomes inside CMMS. This is further confirmed by the widespread uniform spheres (≈ 48.5 nm diameter) observed with cryo-SEM (Figure 5f). Moreover, a reversible pH responsive behavior was verified, comparing the size of CMMS at pH 8 and 5, a larger reversible volume increase of 39% (Figure 5g–j) compared to 21% of SLSP without entrapped polymersomes (Figure 2h–k) is observed.

2.5. Systematic and Adaptive Cell Biomimetics: Hierarchical Multicompartiment Architectures and Enzyme-Mediated, Biological-Responded Transport Behaviors

Above mentioned investigations show the successful construction of polymersomes-in-proteinosome multicompartiment structures, meaning cell-like multicompartimental micro-sized structures (CMMS) without GOx entrapment (Figure 1). In the next step we aimed to simulate certain characteristics of living cells in our CMMS. As a proof of concept, the created CMMS should mimic the characteristics of pancreatic beta cells showing controlled Ins delivery by responding to biological stimuli (glucose). For showing the first dynamic and adaptive processes of the CMMS as cellular biomimetics, we additionally encapsulated the enzyme GOx, leading to a spatially confined glucose-dependent acidic microenvironment for controlling the bio-stimuli-dependent release of Ins from pH-sensitive Psomes-Ins in CMMS.

Again, we used the Pickering emulsion method for encapsulating GOx and Psomes-Ins in SLSP preparing the functional CMMS. As shown before, PEG-Ins release rates from CMMS depend on the pH degrees influenced by the glucose level and GOx activities. In this study, the final concentration of GOx inside CMMS was fixed to be 0.2 mg mL^{-1} in the presence of 10 mg mL^{-1} of glucose. Thus, once the biological pathway biomimetics mediated by the GOx/glucose pair is started, the pH of the solution drops to 5 within 140 min (Figure 6f).

The complete CMMS system was incubated with 0 mg mL^{-1} , 1 mg mL^{-1} (normoglycemic conditions in blood), and 10 mg mL^{-1} (diabetic conditions) of glucose in 10 mM PBS at pH 7.4.^[36] A rapid release of PEG-Ins from CMMS for the highest glucose concentration is observed compared to nearly no release for normoglycemic and no-glucose conditions (Figure 6g). This nearly no-release behavior for normoglycemic and no-glucose conditions over the time (Figure 6g) thoroughly implies that there exists other internally microenvironmental conditions for the located artificial organelles, Psomes-Ins, in the dynamic cytoskeleton-like scaffold of CMMS compared to

the pure release conditions of PEG-Ins from Psomes-Ins under physiological and enzymatic conditions (Figure 4). This also addresses the key parameter of retaining PEG-Ins in artificial organelles characterized by collapsed membranes under neutral blood conditions. Gluconic acid, produced by 1 mg mL^{-1} glucose, also protonates other functional groups of the cytoskeleton-like scaffold of CMMS before protons are involved in the protonation of any artificial organelles' membrane for inducing any release of PEG-Ins from CMMS. This release behavior is congruent to the determined pH drop for CMMS, once produced by GOx in the presence of 1 and 10 mg mL^{-1} of glucose (Figure 6f). At lower glucose concentration, pH drop is down to 6.5 after >350 min. This pH is not suited to induce any significant protonation of artificial organelles' membrane in CMMS for releasing PEG-Ins over 72 h (Figure 6g).

To further investigate the postulated release behavior of PEG-Ins from CMMS above-mentioned, PEG-Ins was labeled with RBITC (red dye; Supporting Information), and the desired release of PEG-Ins from CMMS to external environment was visualized by fluorescence microscopy images of PEG-Ins-loaded CMMS solution and calculating the grey value profiles (Figure 6a–e). Controlled PEG-Ins release from CMMS is undoubtedly observed by varying glucose concentration from 1 to 10 mg mL^{-1} and then decrease back the glucose concentration to 1 mg mL^{-1} (Figure 6h), which is of great interest since it simulates the fluctuant blood glucose level in human body. These first results confirm the expectation of dynamic and adaptive processes in our CMMS as cellular biomimetics.

Moreover, by labeling the polymersome with FITC (green dye, FITC-labeled block copolymer in the Supporting Information), PEG-Ins with RBITC (red dye) and GOx with Cy5 (blue dye), their spatial organization inside the multicompartiment CMMS structure is clearly visualized using confocal laser scanning microscopy of different wavelengths (Figure 7e,f). After incubating CMMS in 10 mg mL^{-1} of glucose solution (containing 10 mM of PBS, pH 7.4) for 24 h, the successful release of the PEG-Ins into the outer aqueous solution (outside CMMS) is observed and without any leakage of the encapsulated GOx and polymersomes acting as artificial organelles (Figure 7e,f). Larger CMMS after addition of glucose (Figure 7f) are observed in opposite to starting CMMS without glucose (Figure 7e). This is in agreement with the release results of PEG-Ins, presented in Figure 6e.

3. Conclusion

In summary, we demonstrated an efficient way to fabricate CMMS (Figure 1) which respond on bio-stimuli by integrating PEG-Ins-loaded polymersomes (Psoemes) and an enzyme, GOx, which produces gluconic acid in the presence of glucose. Especially, the porous protein hydrogel-based cytoskeleton in CMMS plays a key role for the even distribution of Psomes and GOx inside CMMS as well as the enhancement of the structural stability of CMMS. Moreover, the pH-responsive characteristics of both, the protein hydrogel-based cytoskeleton and Psomes, emphasize synergistic acid triggered swelling behaviors of the whole CMMS. Significantly, CMMS provide the possibility of the spatial organization of biological

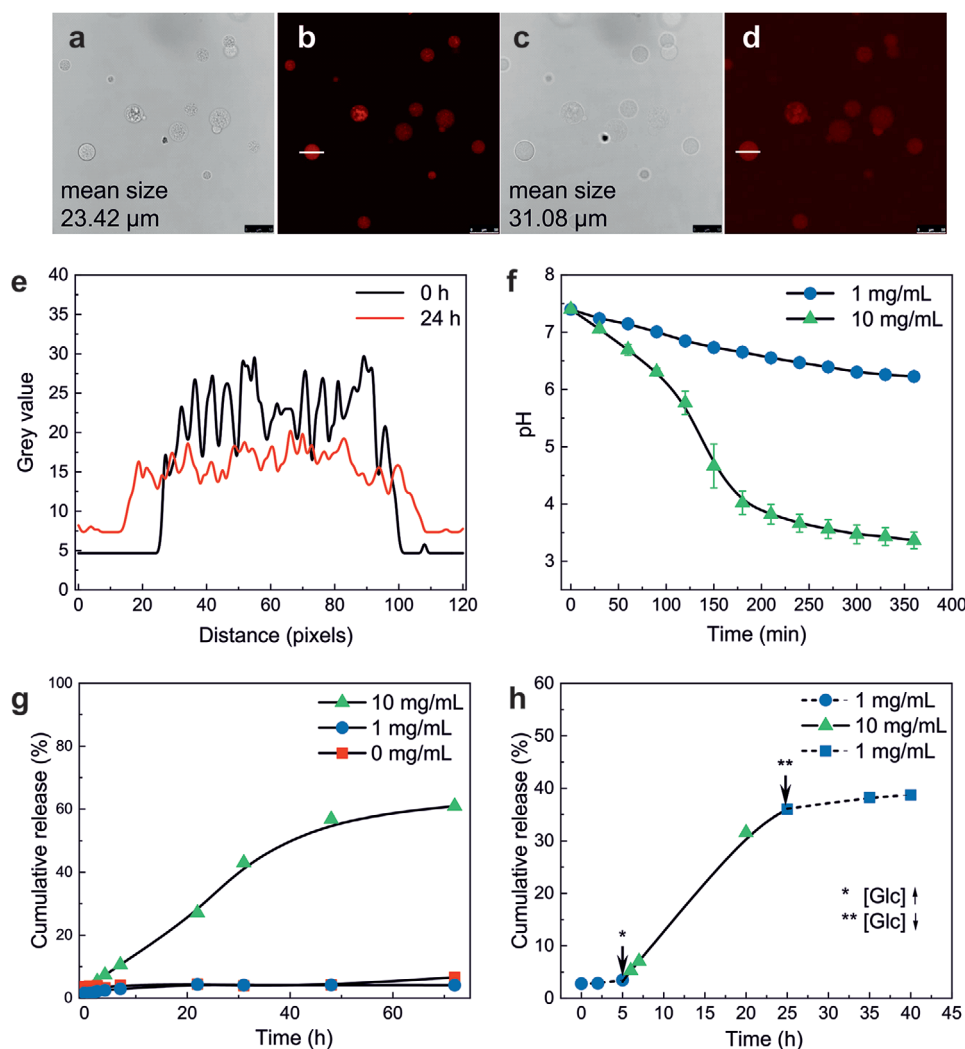


Figure 6. a,b) Optical microscopy images and corresponding confocal laser fluorescence microscopy images of CMMS with integrated Psomes-Ins and GOx and c,d) after incubation for 24 h in 10 mM PBS buffer at pH 7.4 in the presence of 10 mg mL^{-1} glucose solution, using RBITC-labeled PEG-Ins for visualizing PEG-Ins trace in (b and d). Scaling bars are $50 \mu\text{m}$ (a and c). (e) Grey value profiles (intensity profile of fluorescence) of an individual CMMS sphere (with white line as cross-section for analyzing the dimension of CMMS) and the total fluorescence intensity of all loaded RBITC-labeled PEG-Ins for CMMS with Psomes-Ins in (b) and (d)) at 0 and 24 h: fluorescence intensity increases with the incubation time outside of individual CMMS. f) Time dependent enzyme-mediated pH drop of complete CMMS containing 0.2 mg mL^{-1} of GOx in the presence of 1 and 10 mg mL^{-1} of glucose. Data are presented as mean values \pm SD, error bars indicate standard deviations ($n = 3$). g) PEG-Ins release from complete CMMS in the presence of 0, 1, and 10 mg mL^{-1} of glucose. h) Cumulative release of PEG-Ins from complete CMMS with changing glucose concentrations ([Glc]) from 1 to 10 mg mL^{-1} and then decreasing it again to 1 mg mL^{-1} .

(macro)molecules into different microdomains. By the selective loading of GOx into the protein hydrogel-based cytoskeleton domain and PEG-Ins into the pH-sensitive Psomes domain, a glucose-triggered release of PEG-Ins from the constructed CMMS is available at glucose concentrations simulating a diabetic blood level regardless of the outer neutral aqueous environment. Thus, the constructed CMMS imitate pancreatic-like cells in this manner that a specific internal acidic microenvironment of CMMS can be generated from the permanently integrated GOx in the protein hydrogel-based cytoskeleton for converting glucose (=producing protons by gluconic acid) and a constantly permeable outer membrane of CMMS to let diffuse glucose inside the microenvironment

of CMMS. Taken together the advantages of the structural, dynamic, and bio-stimuli feedback controlled characteristics of CMMS, this study emphasizes a new hierarchically multicompartiment platform with orthogonal-responsive membranes. These CMMS have high potential in the field of systems biology for advancing eukaryotic cell biomimetics in basic structures and functionalities.

4. Experimental Section

Preparation and Purification of Psomes-Ins: After adjusting the pH of purified BCP-A solution (10 mL , dissolved in 0.01 M HCl overnight,

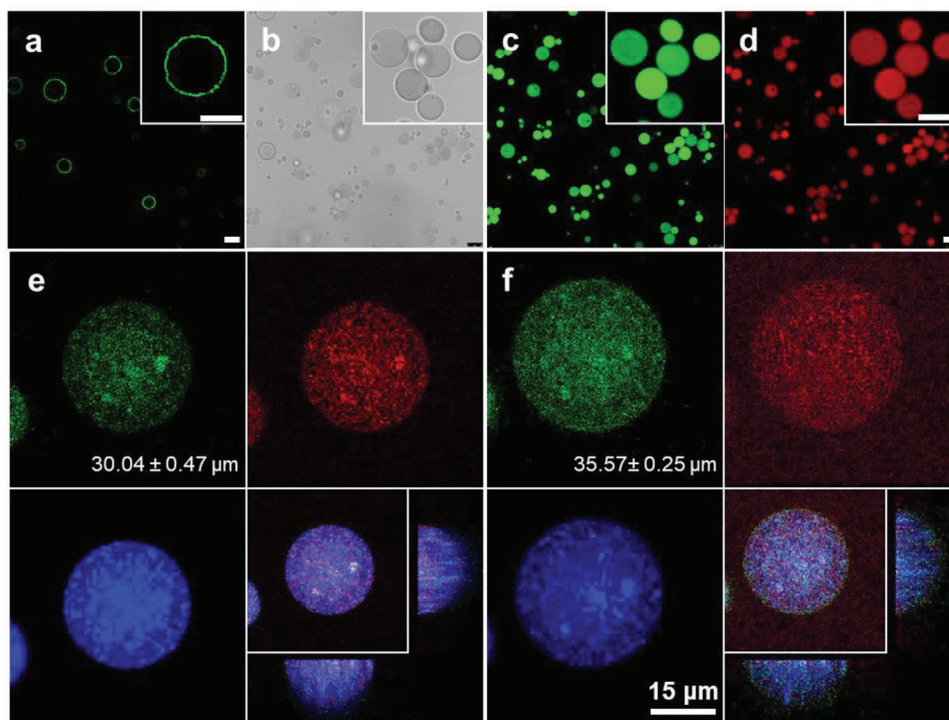


Figure 7. Visualization of different components of CMMS compared with proteinosome and study of stability of GOx in complete CMMS. a) Confocal laser scanning microscopy (CLSM) image of BSA-NH₂-FITC/PNIPAAm proteinosomes (green dye); scale bar is 25 μm. b) Optical microscopy image and c,d) corresponding fluorescence microscopy images of water-in-oil BSA-NH₂-RBITC (red dye = $\lambda_{\text{excitation}}$ 552 nm)/DEX-CHO hydrogel-loaded BSA-NH₂-FITC (green dye = $\lambda_{\text{excitation}}$ 488 nm)/PNIPAAm proteinosomes (for establishing SLSP, skeleton-like scaffold in proteinosomes); scale bars are 25 μm. e) CLSM images of single CMMS sphere at 0 h (10 mM PBS) and f) after 24 h incubation with 10 mg mL⁻¹ glucose solution (10 mM PBS): PEG-Ins labeled with RBITC (red dye = $\lambda_{\text{excitation}}$ 552 nm), Psomes containing BCP-FITC (green dye = $\lambda_{\text{excitation}}$ 488 nm), GOx-Cy5 (blue dye = $\lambda_{\text{excitation}}$ 603 nm) immobilized in SLSP of CMMS. Further details on RBITC labeled PEG-Ins in (e) and (f) are presented in Figure S27, Supporting Information.

1 mg mL⁻¹) to 5.8 which is above the isoelectric point of PEG-Ins and under the Psome self-assembly point, the filtered PEG-Ins aqueous solution (0.2 μm Nylon filter, PEG-Ins at a speed of 200 rpm stirred in 0.05 M Na₂CO₃ for 30 min) was added dropwise into the BCP-A solution and stirred for 30 min. Then mixed solution was continuously adjusted to pH value of ≈8–9 and stirred for 3 days in the dark condition. The next steps were the same procedures as the preparation of Psomes (Supporting Information). For removing the free PEG-Ins not loaded in the Psomes, 10 mL crude Psomes-Ins solution (1 mg mL⁻¹ BCP-A and 0.2 mg mL⁻¹ PEG-Ins) was purified by HFF against 200 mL Milli-Q water (Figure S20, Supporting Information; MWCO: 500 kDa, 130 mbar).

Construction of Protein Hydrogel-Filled Proteinosomes (SLSP): The SLSP was constructed by the same method published in a previous work.^[19] The details are as follows: BSA-NH₂ (7 μL, 200 mg mL⁻¹), sodium phosphate buffer (7 μL, 0.05 M, pH 8), aqueous DEX-CHO (7 μL, 200 mg mL⁻¹), and aqueous NHS-PEG-NHS (5 μL, 1 g mL⁻¹) were added into an aqueous solution containing BSA-NH₂/PNIPAAm conjugates (20 μL, 15 mg mL⁻¹). Then 0.8 mL 2-ethyl-1-hexanol were immediately added into the above mixed solution and shaken for ≈30 s at room temperature to get a uniformly distributed hydrogel-filled proteinosomes. For obtaining a stable SLSP, 5 μL glutaraldehyde (GA) was added into the water-in-oil system. After keeping the solution for 6 h at room temperature, the aqueous SLSP solution was produced by transferring water-in-oil system to aqueous solution (ethanol as the co-solvent, further details in reference 19).

Construction of Psomes/Psomes-Ins-in-Hydrogel-Proteinosomes (CMMS with Psomes or Psomes-Ins, but without GOx): CMMS were fabricated by the Pickering emulsion method same as proteinosomes and hydrogel-filled proteinosomes. BSA-NH₂, DEX-CHO, NHS-PEG-NHS,

and BSA-NH₂/PNIPAAm powders were dissolved in the purified Psomes-Ins aqueous solution (5 mg mL⁻¹, 46 μL) which was condensed by HFF device (1 to 5 mg mL⁻¹, Milli-Q water, MWCO: 500 kDa, 130 mbar), in the same proportion as in the preparation of hydrogel-filled proteinosomes (BSA-NH₂: 200 mg mL⁻¹, DEX-CHO: 200 mg mL⁻¹, NHS-PEG-NHS: 1 g mL⁻¹, and BSA-NH₂/PNIPAAm: 15 mg mL⁻¹ all in 5 mg mL⁻¹ Psomes-Ins aqueous solution). After carrying out the same procedures as for hydrogel-filled proteinosomes, Psome/Psomes-Ins-in-hydrogel-proteinosome was constructed.

Construction of Psomes/Psomes-Ins-in-Hydrogel-Proteinosomes (CMMS with Psomes or Psomes-Ins, with GOx): CMMS with GOx were fabricated by the Pickering emulsion method as mentioned above. The details as follows: 200 mg mL⁻¹ of BSA-NH₂ (7 μL, 5 mg mL⁻¹ Psomes-Ins aqueous solution), 200 mg mL⁻¹ of DEX-CHO (7 μL, 5 mg mL⁻¹ Psomes-Ins aqueous solution), 1 g mL⁻¹ NHS-PEG-NHS (5 μL, 5 mg mL⁻¹ Psomes-Ins aqueous solution), and 100 mg mL⁻¹ of GOx (5 μL, 5 mg mL⁻¹ Psomes-Ins aqueous solution) were added into 15 mg mL⁻¹ of BSA-NH₂/PNIPAAm (20 μL, 5 mg mL⁻¹ Psomes-Ins). After carrying out the same procedures as for CMMS, CMMS with GOx were constructed.

Characterization of Protein Hydrogel-Filled Proteinosomes (SLSP) and Psome/Psomes-Ins-in-Hydrogel-Proteinosome (CMMS with Psomes or Psomes-Ins, but without GOx): The reversible swelling properties of SLSP and CMMS were carried out by measuring their size changes of freshly prepared solutions between pH 5 and pH 8 via optical microscopy. The microscopy images were collected by dropping 10 μL SLSP and CMMS solutions in 0.1 mL pH 8 PBS solution followed by adjusting the solution to pH 5 by 0.1 M HCl addition, and by readjusting to pH 8 by 0.1 M NaOH addition and vice versa (1.5% and 1% GA shown in Figure S21, Supporting Information).

PEG-Ins Release Kinetics from Psomes-Ins and CMMS (with Psomes-Ins and GOx): 3×5 mL Psomes-Ins stock solutions (0.2 mg mL^{-1}) were dialyzed at 1 L PBS buffer (10 mM) pH 7.4, 6.5, and 5.5 respectively over 3 days. Besides, 3×5 mL Psomes-Ins stock solutions (0.2 mg mL^{-1}) were respectively dialyzed in 1 L PBS buffers (10 mM) with the addition of 0, 1, and 10 mg mL^{-1} gluconic acid over 2 days. Finally, for imitating the PEG-Ins release from CMMS (Figure 1) triggered by enzyme reaction, 2 mL Psomes-Ins stock solution (1 mg mL^{-1}) was dialyzed in 100 mL PBS buffer (10 mM, with glucose (10 mg mL^{-1}) and GOx (0.2 mg mL^{-1}) addition).

PEG-Ins release kinetics from the complete CMMS (Figure 1) were realized by respectively incubating the 300 μL Psomes-Ins-in-hydrogel-proteinosome aqueous solutions (concentration of above mentioned fabrication steps) in 15 mL of 10 mM PBS buffers with the addition of glucose at concentrations of 0, 1, and 10 mg mL^{-1} . After transferring 1 mL mixed solutions and picking the upper solutions via centrifuging process at different time, the PEG-Ins release curves were calculated by testing the fluorescence intensity. The PEG-Ins release curve from complete CMMS (Figure 1) with changing glucose concentration was carried out in the same way (Figure 6h). However, the release trend changed during the incubation period with increasing (by directly adding glucose into release solution after 5 h incubation in 10 mM PBS glucose at 1 mg mL^{-1} concentration) or decreasing (by removing the upper release solution and adding fresh 1 mg mL^{-1} concentration 10 mM PBS glucose) glucose concentrations between 1 and 10 mg mL^{-1} .

All the release profiles were obtained by measuring the fluorescence intensity of dialysis solutions. Especially for the PEG-Ins release from CMMS, the above fluorescence intensity curves and control experiment curves were collected at $\lambda_{\text{Em}} = 575 \text{ nm}$ ($\lambda_{\text{Ex}} = 535 \text{ nm}$, Figure S22, Supporting Information).

Supporting Information

Supporting Information is available from the Wiley Online Library or from the author.

Acknowledgements

X.H. is grateful for the financial support from NSFC (21871069 and 21474025); P.W. is grateful for a scholarship under the Chinese government award for outstanding students abroad by the China Scholarship Council (CSC). The authors thank the Chair of Botany (C. Neinhuis) at the faculty of Biology of TU Dresden, Germany, for providing equipment and access to cryo-SEM/EDX.

Open access funding enabled and organized by Projekt DEAL.

Conflict of Interest

The authors declare no conflict of interest.

Keywords

biological responses, cell engineering, multicompartment, polymersomes, proteinosomes

Received: September 15, 2020

Revised: November 13, 2020

Published online: December 29, 2020

[1] J. W. Szostak, D. P. Bartel, P. L. Luisi, *Nature* **2001**, 409, 387.

[2] D. A. Fletcher, R. D. Mullins, *Nature* **2010**, 463, 485.

- [3] H. Choi, C. D. Montemagno, *Nano Lett.* **2005**, 5, 2538.
 [4] J. Gaitzsch, X. Huang, B. Voit, *Chem. Rev.* **2016**, 116, 1053.
 [5] J. Liu, V. Postupalenko, S. Lörcher, D. L. Wu, M. Chami, W. Meier, C. G. Palivan, *Nano Lett.* **2016**, 16, 7128.
 [6] a) B. C. Buddingh', J. C. M. van Hest, *Acc. Chem. Res.* **2017**, 50, 769; b) D. A. Hammer, N. P. Kamat, F. Lett, *FEBS Lett.* **2012**, 586, 2882.
 [7] a) S. Deshpande, C. Dekker, *Nat. Protoc.* **2018**, 13, 856; b) A. N. Wang, J. W. Szostak, *Emerging Top. Life Sci.* **2019**, 3, 537.
 [8] M. Li, X. Huang, S. Mann, *Small* **2014**, 10, 3291.
 [9] a) T. Y. D. Tang, C. R. C. Hak, A. J. Thompson, M. K. Kuimova, D. S. Williams, A. W. Perriman, S. Mann, *Nat. Chem.* **2014**, 6, 527; b) J. B. Li, X. M. Liu, L. K. Abdelmohsen, D. S. Williams, X. Huang, *Small* **2019**, 15, 1902893.
 [10] a) X. Huang, M. Li, D. C. Green, D. S. Williams, A. J. Patil, S. Mann, *Nat. Commun.* **2013**, 4, 2239; b) X. L. Wang, X. M. Liu, X. Huang, *Adv. Mater.* **2020**, 32, 2001436; c) L. Wang, S. D. Song, J. van Hest, L. K. Abdelmohsen, X. Huang, S. Sánchez, *Small* **2020**, 16, 1907680.
 [11] Q. Shao, S. D. Zhang, Z. Hu, Y. F. Zhou, *Angew. Chem., Int. Ed.* **2020**, 59, 17125.
 [12] X. Yan, T. T. Wang, D. Yao, J. Y. Xu, Q. Luo, J. Q. Liu, *Small* **2019**, 15, 1900350.
 [13] M. Marguet, C. Bonduelle, S. Lecommandoux, *Chem. Soc. Rev.* **2013**, 42, 512.
 [14] H. X. Chen, W. R. Li, Y. P. Lin, L. Wang, X. M. Liu, X. Huang, *Angew. Chem., Int. Ed.* **2020**, 59, 16953.
 [15] A. Armada-Moreira, E. Taipaleenmäki, F. Itef, Y. Zhang, B. Städler, *Nanoscale* **2016**, 8, 19510.
 [16] X. L. Liu, D. Appelhans, B. Voit, *J. Am. Chem. Soc.* **2018**, 140, 16106.
 [17] N. Martin, M. Li, S. Mann, *Langmuir* **2016**, 32, 5881.
 [18] X. Huang, A. J. Patil, M. Li, S. Mann, *J. Am. Chem. Soc.* **2014**, 136, 9225.
 [19] P. Wen, X. M. Liu, L. Wang, M. Li, Y. D. Huang, X. Huang, S. Mann, *Small* **2017**, 13, 1700467.
 [20] L. Rodríguez-Arco, M. Li, S. Mann, *Nat. Mater.* **2017**, 16, 857.
 [21] Y. Qiao, M. Li, R. Booth, S. Mann, *Nat. Chem.* **2017**, 9, 110.
 [22] C. Y. Zhao, M. Zhu, Y. Fang, X. M. Liu, L. Wang, D. F. Chen, X. Huang, *Mater. Horiz.* **2020**, 7, 157.
 [23] A. Belluati, S. Thambo, A. Najer, V. Maffei, P. von Claudio, I. Craciun, C. G. Palivan, W. Meier, *Adv. Funct. Mater.* **2020**, 30, 2002949.
 [24] X. M. Liu, P. Zhou, Y. D. Huang, M. Li, X. Huang, S. Mann, *Angew. Chem., Int. Ed.* **2016**, 55, 7095.
 [25] S. Mann, *Acc. Chem. Res.* **2011**, 45, 2131.
 [26] P. Schwille, J. Spatz, K. Landfester, E. Bodenschatz, S. Herminghaus, V. Sourjik, T. J. Erb, P. Bastiaens, R. Lipowsky, A. Hyman, P. Dabrock, J. C. Baret, T. Vidakovic-Koch, P. Bieling, R. Dimova, H. Mutschler, T. Robinson, T. Y. D. Tang, S. Wegner, K. Sundmacher, *Angew. Chem., Int. Ed.* **2018**, 57, 13382.
 [27] L. Wang, Y. P. Lin, Y. T. Zhou, H. Xie, S. J. M. M. Li, Y. D. Huang, X. Huang, S. Mann, *Angew. Chem., Int. Ed.* **2019**, 58, 1067.
 [28] P. Y. Bolinger, D. Stamou, H. Vogel, *Angew. Chem., Int. Ed.* **2008**, 47, 5544.
 [29] Z. P. Wang, M. C. van Oers, F. P. Rutjes, J. C. van Hest, *Angew. Chem., Int. Ed.* **2012**, 51, 10746.
 [30] P. Gobbo, A. J. Patil, M. Li, R. Harniman, W. H. Briscoe, S. Mann, *Nat. Mater.* **2018**, 17, 1145.
 [31] A. Peyret, E. Ibarboure, N. Pippa, S. Lecommandoux, *Langmuir* **2017**, 33, 7079.
 [32] A. F. Mason, N. A. Yewdall, P. L. W. Welzen, J. X. Shao, M. van Stevendael, J. C. M. van Hest, D. S. Williams, L. K. Abdelmohsen, *ACS Cent. Sci.* **2019**, 5, 1360.
 [33] X. L. Liu, P. Formanek, B. Voit, D. Appelhans, *Angew. Chem., Int. Ed.* **2017**, 56, 16233.
 [34] J. Gaitzsch, D. Appelhans, L. G. Wang, G. Battaglia, B. Voit, *Angew. Chem., Int. Ed.* **2012**, 51, 4448.

- [35] M. J. Webber, E. A. Appel, B. Vinciguerra, A. B. Cortinas, L. S. Thapa, S. Jhunjhunwala, L. Isaacs, R. Langer, D. G. Anderson, *Proc. Natl. Acad. Sci. USA* **2016**, *113*, 14189.
- [36] D. H. Chou, M. J. Webber, B. C. Tang, A. B. Lin, L. S. Thapa, D. Deng, J. V. Truong, A. B. Cortinas, R. Langer, D. G. Anderson, *Proc. Natl. Acad. Sci. USA* **2015**, *112*, 2401.
- [37] Y. Z. Gao, Q. Luo, S. P. Qiao, L. Wang, Z. Y. Dong, J. Y. Xu, J. Q. Liu, *Angew. Chem., Int. Ed.* **2014**, *53*, 9343.
- [38] D. Y. Su, X. M. Liu, L. Wang, C. Ma, H. Xie, H. Zhang, X. H. Meng, Y. D. Huang, X. Huang, *Chem. Commun.* **2016**, *52*, 13803.
- [39] H. Gumz, S. Boye, B. Iyisan, V. Krönert, P. Formanek, B. Voit, A. Lederer, D. Appelhans, *Adv. Sci.* **2019**, *6*, 1801299.
- [40] D. Gräfe, J. Gaitzsch, D. Appelhans, B. Voit, *Nanoscale* **2014**, *6*, 10752.
- [41] M. A. Yassin, D. Appelhans, R. Wiedemuth, P. Formanek, S. Boye, A. Lederer, A. Temme, B. Voit, *Small* **2015**, *11*, 1580.
- [42] B. Iyisan, J. Kluge, P. Formanek, B. Voit, D. Appelhans, *Chem. Mater.* **2016**, *28*, 1513.
- [43] H. Gumz, T. H. Lai, B. Voit, D. Appelhans, *Polym. Chem.* **2017**, *8*, 2904.
- [44] K. Hinds, J. J. Koh, L. Joss, F. Liu, M. Baudys, S. W. Kim, *Bioconjugate Chem.* **2000**, *11*, 195.
- [45] S. Chen, J. L. Qin, J. Z. Du, *Macromolecules* **2020**, *53*, 3978.
- [46] L. D. Blackman, S. Varlas, M. C. Arno, Z. H. Houston, N. L. Fletcher, K. J. Thurecht, M. Hasan, M. I. Gibson, R. K. O'Reilly, *ACS Cent. Sci.* **2018**, *4*, 718.
- [47] C. G. Palivan, O. Fischer-Onaca, M. Delcea, F. IteI, W. Meier, *Chem. Soc. Rev.* **2012**, *41*, 2800.
- [48] B. Iyisan, A. C. Siedel, H. Gumz, M. Yassin, J. Kluge, J. Gaitzsch, P. Formanek, S. Moreno, B. Voit, D. Appelhans, *Macromol. Rapid Commun.* **2017**, *38*, 1700486.
- [49] M. Garni, S. Thamboo, C.-A. Schoenenberger, C. G. Palivan, *Biochim. Biophys. Acta, Biomembr.* **2017**, *1859*, 619.
- [50] S. Moreno, P. Sharan, J. Engelke, H. Gumz, U. Oertel, B. Voit, S. Banerjee, R. Klajn, P. Wang, A. Lederer, D. Appelhans, *Small* **2020**, *16*, 2002135.